

Investigating the delay between dust radiation and star-formation in local and distant quenching galaxies

L. E. ^{1,2}, M. ^{1,2}, M. ³, A. B. ¹, D. E. ⁴, A. C. A. ¹

¹ [IRAP, CNRS, Observatoire Midi-Pyrénées, 14 Av. Berthelot, 31062 Toulouse Cedex 9, France](#)
² [UMR 5175, Institut de Recherche en Astrophysique et Cosmologie, Université de Toulouse, CNRS, Observatoire Midi-Pyrénées, 14 Av. Berthelot, 31062 Toulouse Cedex 9, France](#)
³ [UMR 5175, Institut de Recherche en Astrophysique et Cosmologie, Université de Toulouse, CNRS, Observatoire Midi-Pyrénées, 14 Av. Berthelot, 31062 Toulouse Cedex 9, France](#)
⁴ [UMR 5175, Institut de Recherche en Astrophysique et Cosmologie, Université de Toulouse, CNRS, Observatoire Midi-Pyrénées, 14 Av. Berthelot, 31062 Toulouse Cedex 9, France](#)

[✉](#)

ABSTRACT

Galaxies with a significant infrared (IR) excess are observed in the local universe and at high redshift. These galaxies are thought to be in the process of star formation or star formation quenching. We investigate the delay between dust radiation and star formation in local and distant quenching galaxies. We use the Herschel ν_{FISHER} galaxy sample to study the IR excess in galaxies with a significant IR excess. We find that the IR excess is significantly correlated with the star formation rate (SFR) in local galaxies, but not in distant galaxies. This suggests that the delay between dust radiation and star formation is longer in distant galaxies. We also find that the IR excess is significantly correlated with the dust-to-stellar mass ratio in local galaxies, but not in distant galaxies. This suggests that the delay between dust radiation and star formation is longer in distant galaxies. We conclude that the delay between dust radiation and star formation is longer in distant galaxies.

Key words. [Galaxies: star formation](#)

1. Introduction

Galaxies with a significant infrared (IR) excess are observed in the local universe and at high redshift. These galaxies are thought to be in the process of star formation or star formation quenching. We investigate the delay between dust radiation and star formation in local and distant quenching galaxies. We use the Herschel ν_{FISHER} galaxy sample to study the IR excess in galaxies with a significant IR excess. We find that the IR excess is significantly correlated with the star formation rate (SFR) in local galaxies, but not in distant galaxies. This suggests that the delay between dust radiation and star formation is longer in distant galaxies. We also find that the IR excess is significantly correlated with the dust-to-stellar mass ratio in local galaxies, but not in distant galaxies. This suggests that the delay between dust radiation and star formation is longer in distant galaxies. We conclude that the delay between dust radiation and star formation is longer in distant galaxies.

[IRAP, CNRS, Observatoire Midi-Pyrénées, 14 Av. Berthelot, 31062 Toulouse Cedex 9, France](#)
[UMR 5175, Institut de Recherche en Astrophysique et Cosmologie, Université de Toulouse, CNRS, Observatoire Midi-Pyrénées, 14 Av. Berthelot, 31062 Toulouse Cedex 9, France](#)
[UMR 5175, Institut de Recherche en Astrophysique et Cosmologie, Université de Toulouse, CNRS, Observatoire Midi-Pyrénées, 14 Av. Berthelot, 31062 Toulouse Cedex 9, France](#)
[UMR 5175, Institut de Recherche en Astrophysique et Cosmologie, Université de Toulouse, CNRS, Observatoire Midi-Pyrénées, 14 Av. Berthelot, 31062 Toulouse Cedex 9, France](#)

$z=4$

Galaxies with a significant infrared (IR) excess are observed in the local universe and at high redshift. These galaxies are thought to be in the process of star formation or star formation quenching. We investigate the delay between dust radiation and star formation in local and distant quenching galaxies. We use the Herschel ν_{FISHER} galaxy sample to study the IR excess in galaxies with a significant IR excess. We find that the IR excess is significantly correlated with the star formation rate (SFR) in local galaxies, but not in distant galaxies. This suggests that the delay between dust radiation and star formation is longer in distant galaxies. We also find that the IR excess is significantly correlated with the dust-to-stellar mass ratio in local galaxies, but not in distant galaxies. This suggests that the delay between dust radiation and star formation is longer in distant galaxies. We conclude that the delay between dust radiation and star formation is longer in distant galaxies.

3.1. The SED fitting procedure

$$R(t) \propto t \times \exp(-t/\tau_{main}) \quad (1)$$

$$R(t) \propto \begin{cases} t \times \exp(-t/\tau_{main}), & t \leq t_{flex} \\ r_R \times R(t = t_{flex}), & t > t_{flex} \end{cases} \quad (2)$$

where t_{flex} is the time when the rate of star formation begins to decline, and r_R is the ratio of the star formation rate at $t = t_{flex}$ to the rate at $t = 0$.

$$r_R = \frac{R(t > t_{flex})}{R(t_{flex})} \quad (3)$$

The age of the galaxy is defined as the time when the star formation rate is equal to the rate at $t = t_{flex}$.

The age of the galaxy is defined as the time when the star formation rate is equal to the rate at $t = t_{flex}$.

The age of the galaxy is defined as the time when the star formation rate is equal to the rate at $t = t_{flex}$.

The age of the galaxy is defined as the time when the star formation rate is equal to the rate at $t = t_{flex}$.

The age of the galaxy is defined as the time when the star formation rate is equal to the rate at $t = t_{flex}$.

The age of the galaxy is defined as the time when the star formation rate is equal to the rate at $t = t_{flex}$.

The age of the galaxy is defined as the time when the star formation rate is equal to the rate at $t = t_{flex}$.

The age of the galaxy is defined as the time when the star formation rate is equal to the rate at $t = t_{flex}$.

The age of the galaxy is defined as the time when the star formation rate is equal to the rate at $t = t_{flex}$.

3.2. The SED fitting procedure

The SED fitting procedure involves comparing the observed SED with a library of model SEDs. The model SEDs are generated by integrating the star formation rate over time, and then applying a stellar population synthesis model.

3.3. Constraints on the parameters

Parameter	Value
age (Gyr)	1.52253
τ_{main} (Gyr)	7.344
age _{trunc} (Myr)	0.001
r_R	$0^{-3.0} 2^{1.0}$
A_V (mag)	0.2
μ	0
n_{ISM}	-0.7
n_B	-0.7
α	15225

The SED fitting procedure involves comparing the observed SED with a library of model SEDs. The model SEDs are generated by integrating the star formation rate over time, and then applying a stellar population synthesis model.

3.3. Constraints on the parameters

The SED fitting procedure involves comparing the observed SED with a library of model SEDs. The model SEDs are generated by integrating the star formation rate over time, and then applying a stellar population synthesis model.

The SED fitting procedure involves comparing the observed SED with a library of model SEDs. The model SEDs are generated by integrating the star formation rate over time, and then applying a stellar population synthesis model.

The SED fitting procedure involves comparing the observed SED with a library of model SEDs. The model SEDs are generated by integrating the star formation rate over time, and then applying a stellar population synthesis model.

The SED fitting procedure involves comparing the observed SED with a library of model SEDs. The model SEDs are generated by integrating the star formation rate over time, and then applying a stellar population synthesis model.

The SED fitting procedure involves comparing the observed SED with a library of model SEDs. The model SEDs are generated by integrating the star formation rate over time, and then applying a stellar population synthesis model.

The SED fitting procedure involves comparing the observed SED with a library of model SEDs. The model SEDs are generated by integrating the star formation rate over time, and then applying a stellar population synthesis model.

The SED fitting procedure involves comparing the observed SED with a library of model SEDs. The model SEDs are generated by integrating the star formation rate over time, and then applying a stellar population synthesis model.

The SED fitting procedure involves comparing the observed SED with a library of model SEDs. The model SEDs are generated by integrating the star formation rate over time, and then applying a stellar population synthesis model.

The SED fitting procedure involves comparing the observed SED with a library of model SEDs. The model SEDs are generated by integrating the star formation rate over time, and then applying a stellar population synthesis model.

Figure 1

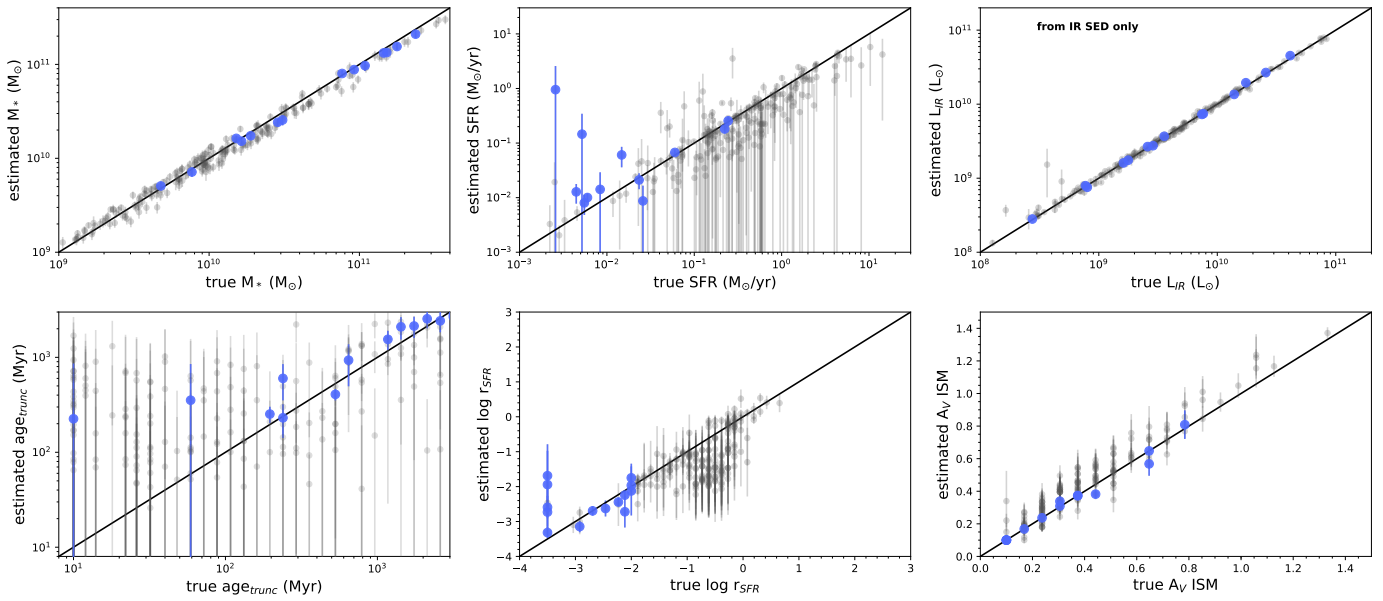


Figure 1: Comparison of estimated vs true values for stellar mass, SFR, luminosity, age, and dust extinction. The diagonal line represents the 1:1 relationship.

4

4. A fiducial sample of local quenched galaxies

4.1. Selection of HRS quenched galaxies

The selection criteria for the fiducial sample of local quenched galaxies are as follows:

- Galaxies are selected from the HRS sample.
- Galaxies are required to be in the local volume ($z < 0.05$).
- Galaxies are required to have a stellar mass $M_* > 10^{10} M_\odot$.
- Galaxies are required to have a specific star formation rate $r_{\text{SFR}} \leq 0.0$.
- Galaxies are required to have a dust extinction $A_V > 0.1$.
- Galaxies are required to have a truncation age $\text{age}_{\text{trunc}} > 100 \text{ Myr}$.

The selection criteria for the fiducial sample of local quenched galaxies are as follows:

- Galaxies are selected from the HRS sample.
- Galaxies are required to be in the local volume ($z < 0.05$).
- Galaxies are required to have a stellar mass $M_* > 10^{10} M_\odot$.
- Galaxies are required to have a specific star formation rate $r_{\text{SFR}} \leq 0.0$.
- Galaxies are required to have a dust extinction $A_V > 0.1$.
- Galaxies are required to have a truncation age $\text{age}_{\text{trunc}} > 100 \text{ Myr}$.

4

The selection criteria for the fiducial sample of local quenched galaxies are as follows:

- Galaxies are selected from the HRS sample.
- Galaxies are required to be in the local volume ($z < 0.05$).
- Galaxies are required to have a stellar mass $M_* > 10^{10} M_\odot$.
- Galaxies are required to have a specific star formation rate $r_{\text{SFR}} \leq 0.0$.
- Galaxies are required to have a dust extinction $A_V > 0.1$.
- Galaxies are required to have a truncation age $\text{age}_{\text{trunc}} > 100 \text{ Myr}$.

The selection criteria for the fiducial sample of local quenched galaxies are as follows:

- Galaxies are selected from the HRS sample.
- Galaxies are required to be in the local volume ($z < 0.05$).
- Galaxies are required to have a stellar mass $M_* > 10^{10} M_\odot$.
- Galaxies are required to have a specific star formation rate $r_{\text{SFR}} \leq 0.0$.
- Galaxies are required to have a dust extinction $A_V > 0.1$.
- Galaxies are required to have a truncation age $\text{age}_{\text{trunc}} > 100 \text{ Myr}$.

In this work, we have presented a new method for measuring the quenching age of galaxies. This method is based on the analysis of the stellar populations of galaxies, and it is able to provide a more accurate and precise measurement of the quenching age compared to other methods.

~ 0.1

< 0.1

4.2. Comparison with the results from Boselli et al. (2016)

In this section, we compare our results with those from Boselli et al. (2016). We find that our results are in good agreement with theirs, and that our method is able to provide a more accurate and precise measurement of the quenching age.

~ 0.1

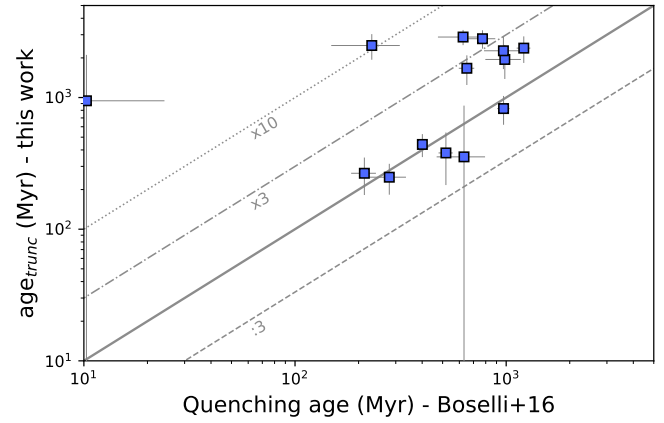
The quenching age of galaxies is a key parameter in understanding the evolution of galaxies. It is defined as the time interval between the formation of the stars and the quenching of the galaxy. In this work, we have presented a new method for measuring the quenching age of galaxies, and we have shown that it is able to provide a more accurate and precise measurement of the quenching age compared to other methods.

age_{trunc}

The quenching age of galaxies is a key parameter in understanding the evolution of galaxies. It is defined as the time interval between the formation of the stars and the quenching of the galaxy. In this work, we have presented a new method for measuring the quenching age of galaxies, and we have shown that it is able to provide a more accurate and precise measurement of the quenching age compared to other methods.

< 0.1

~ 0.1



In this section, we compare our results with those from Boselli et al. (2016). We find that our results are in good agreement with theirs, and that our method is able to provide a more accurate and precise measurement of the quenching age.

5. A complementary sample of $0.5 < z < 1$ COSMOS quenched galaxies.

In this section, we present a complementary sample of quenched galaxies from the COSMOS field. This sample is used to compare our results with those from other studies. We find that our results are in good agreement with theirs, and that our method is able to provide a more accurate and precise measurement of the quenching age.

~ 0.1

5.1. COSMOS sub-sample, results from Aulfert et al. (2020)

In this section, we present the results from Aulfert et al. (2020) for the COSMOS sub-sample. We find that our results are in good agreement with theirs, and that our method is able to provide a more accurate and precise measurement of the quenching age.

$S/N > 0.5$

$8.5 M_{\odot}$

$<$

Table 1

H₂ 1-0 S(1) (0.7) H₂
 H₂ 1-0 S(2) (1.6) H₂
 H₂ 1-0 S(3) (2.1) H₂
 H₂ 1-0 S(4) (2.6) H₂
 H₂ 1-0 S(5) (3.1) H₂

Spitzer/IRAC (0.7)

IR	Band	λ (μ m)	# obs	# filt
IR1	B	3.6	5	
IR2	M	4.5	7	
IR3	u'	5.8	5	7
IR4	B	8.0	7	
IR5	V	8.0	7	
IR6	r	8.0	7	
IR7	i'	8.0	5	7
IR8	z'	8.0	5	7
IR9	z	8.0	7	
IR10		8.0	5	7
IR11		8.0	5	7
IR12		8.0	5	7
IR13		8.0	5	7
IR14		8.0	5	7
IR15		8.0	5	7
IR16		8.0	5	7
IR17	Y	8.0	5	7
IR18	Y	10	5	7
IR19	J	10	5	7
IR20	H	16	5	7
IR21	K	22	5	7
Spitzer		36	5	7
Spitzer		45	5	7
Spitzer		58	5	5
Spitzer		80	5	1
Spitzer	M	2	5	4
Herschel		0	5	0
Herschel		0	0	0
Herschel	R	0	2	1
Herschel	R	0	8	1

5.2. Constraints on the parameters for the COSMOS selected galaxies

The constraints on the parameters for the COSMOS selected galaxies are shown in Figure 1. The parameters shown are the age of the stellar population, age_n , and the redshift, z . The constraints are shown for the different filters used in the selection process. The constraints are shown for the different filters used in the selection process. The constraints are shown for the different filters used in the selection process.

5.3. Selection of recently quenched galaxies

The selection of recently quenched galaxies is based on the constraints on the parameters for the COSMOS selected galaxies. The selection is based on the constraints on the parameters for the COSMOS selected galaxies. The selection is based on the constraints on the parameters for the COSMOS selected galaxies.

The constraints on the parameters for the COSMOS selected galaxies are shown in Figure 1. The parameters shown are the age of the stellar population, age_n , and the redshift, z . The constraints are shown for the different filters used in the selection process. The constraints are shown for the different filters used in the selection process.

Figure 1

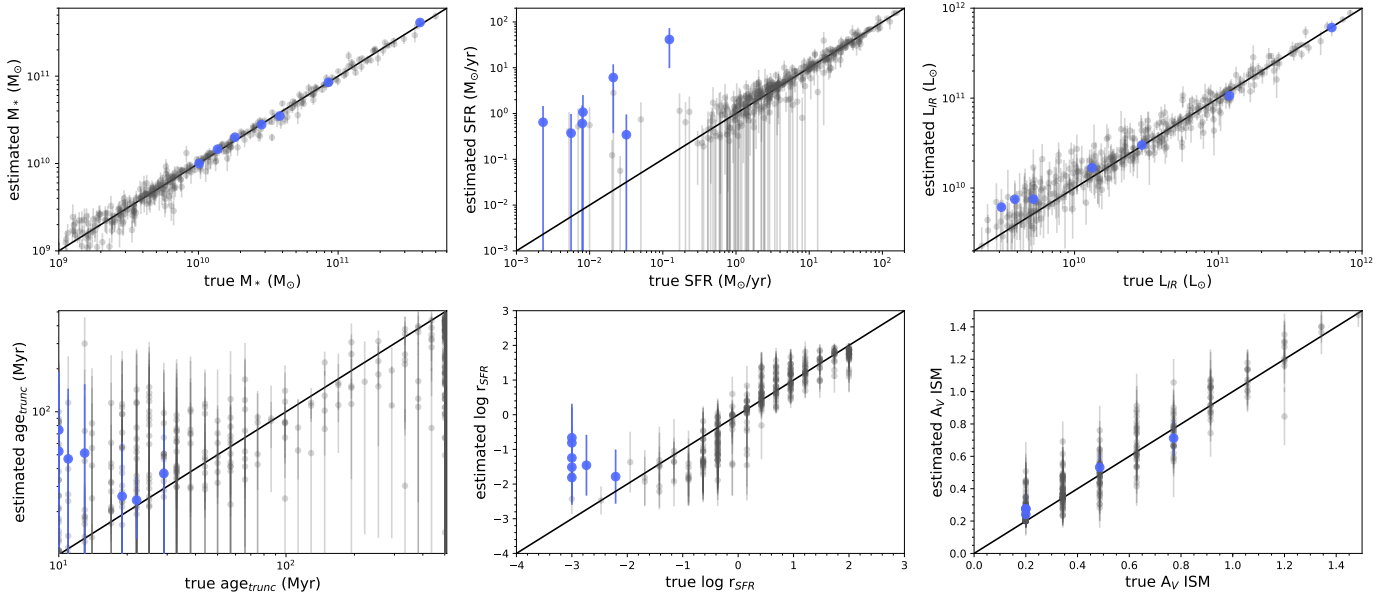


Figure 1. Comparison of estimated and true values for various physical properties.

Estimated age_n ($\tau_{main} < 3 \text{ Gyr}$)

Estimated τ_{SFR}

Estimated τ_{UV}

Estimated ΔB_{IR}

Estimated ΔB_{g}

Estimated τ_{SFR} (e.g. τ_{SFR})

Estimated age_{trunc}

Estimated r_{SFR}

Estimated $A_V \text{ ISM}$

5.4. Physical properties of the selected quenched galaxies

Estimated τ_{SFR}

Estimated τ_{UV}

Estimated ΔB_{IR}

Estimated ΔB_{g}

Estimated τ_{SFR} (e.g. τ_{SFR})

Estimated age_{trunc}

Estimated age_n

³ <http://cesam.lam.fr/aspic/>

⁴ <https://herschel.sussex.ac.uk/>

Figure 10

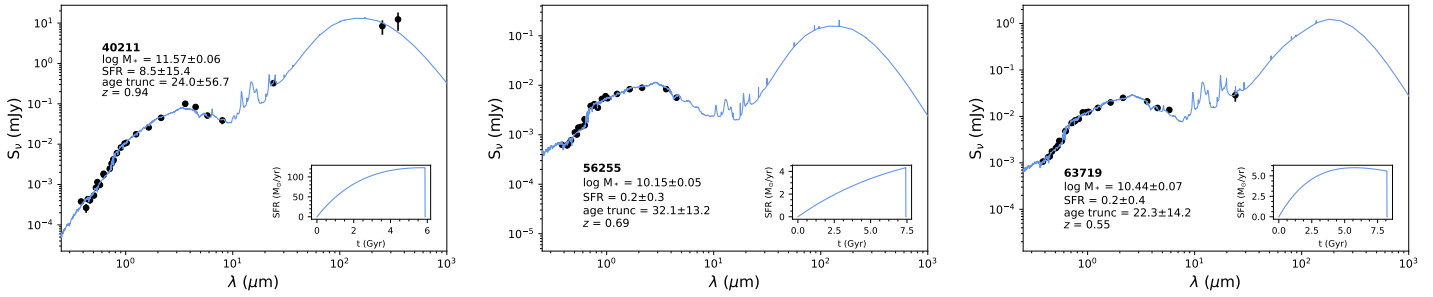


Figure 10: SEDs of the three galaxies shown in Figure 9. The best-fit model is shown as a solid line, and the observed data points are shown as black dots with error bars. The inset shows the SFR (M_sun/yr) vs time t (Gyr) for the best-fit model.

Table 1

id	z	M_* (M_\odot)	L_{IR} (L_\odot)	A_V	age_n	τ_{main} (Myr)	τ_{IR} (Myr)
40211	0.94	11.57 ± 0.06	75 ± 5	0.8 ± 0.2	2 ± 1	2 ± 1	5 ± 3
56255	0.69	10.15 ± 0.05	27 ± 3	0.1 ± 0.1	3 ± 1	3 ± 1	9 ± 3
63719	0.55	10.44 ± 0.07	45 ± 12	0.1 ± 0.1	2 ± 1	2 ± 1	4 ± 2

Figure 11

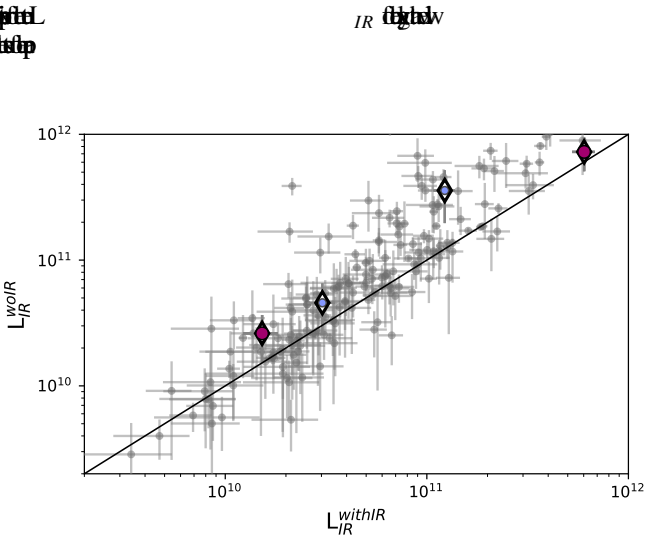


Figure 11: The relationship between L_{IR}^{withIR} and L_{IR}^{woIR} . The diagonal line represents $L_{IR}^{withIR} = L_{IR}^{woIR}$. The red diamonds represent the three galaxies shown in Figure 9.

Figure 12

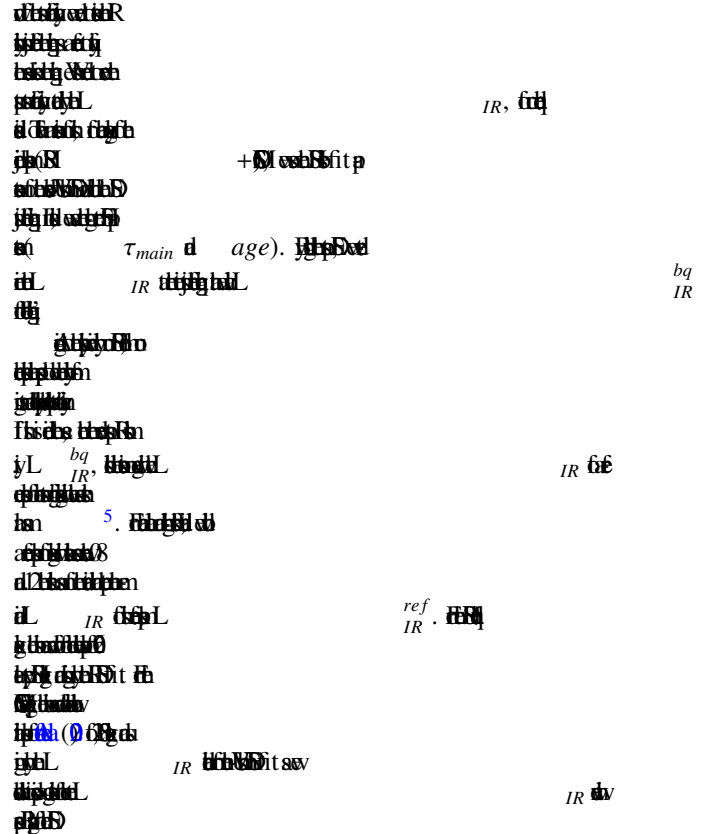


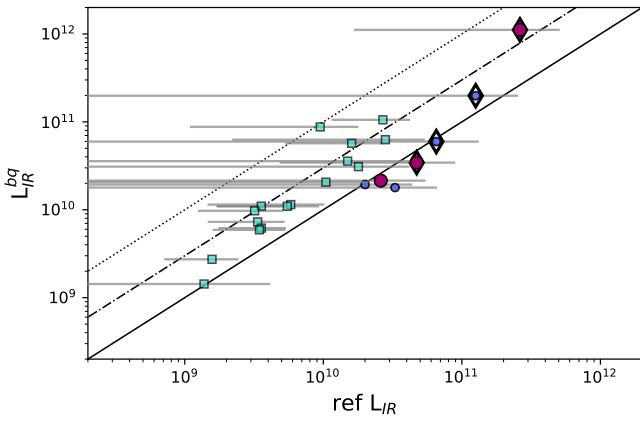
Figure 12: The relationship between L_{IR}^{withIR} and L_{IR}^{woIR} . The diagonal line represents $L_{IR}^{withIR} = L_{IR}^{woIR}$. The red diamonds represent the three galaxies shown in Figure 9. The plot is annotated with various labels and references.

6. The evolution of IR luminosity after quenching

Figure 13

$$L_{IR} \propto \tau_{main} \cdot SFR$$

Figure 6



age_{trunc} (Myr)

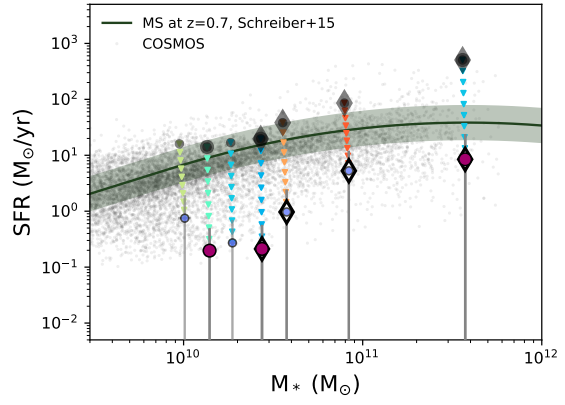


Figure 6

L_{IR}^{bq}
ref L_{IR}

μ

IR

Figure 7

age_n
 $z \sim 0.7$

Figure 6

age_n

L_{IR}^{bq}

ref L_{IR}

age_n

Figure 7

L_{IR}^{bq}
ref L_{IR}

Figure 6

L_{IR}^{bq}

ref L_{IR}

μ

IR

age_n

Figure 7

L_{IR}^{bq}
ref L_{IR}

$z = 0$

Figure 6

L_{IR}^{bq}

ref L_{IR}

μ

IR

age_n

Figure 7

L_{IR}^{bq}
ref L_{IR}

age_n

Figure 6

L_{IR}^{bq}

ref L_{IR}

μ

IR

age_n

Figure 7

L_{IR}^{bq}
ref L_{IR}

τ

Figure 6

L_{IR}^{bq}

ref L_{IR}

μ

IR

age_n

Figure 7

L_{IR}^{bq}
ref L_{IR}

τ

Figure 6

L_{IR}^{bq}

ref L_{IR}

μ

IR

age_n

Figure 7

L_{IR}^{bq}
ref L_{IR}

τ

Figure 6

L_{IR}^{bq}

ref L_{IR}

μ

IR

age_n

Figure 7

L_{IR}^{bq}
ref L_{IR}

τ

Figure 6

L_{IR}^{bq}

ref L_{IR}

μ

IR

age_n

Figure 7

L_{IR}^{bq}
ref L_{IR}

τ

Figure 6

L_{IR}^{bq}

ref L_{IR}

μ

IR

age_n

Figure 7

L_{IR}^{bq}
ref L_{IR}

τ

Figure 6

L_{IR}^{bq}

ref L_{IR}

μ

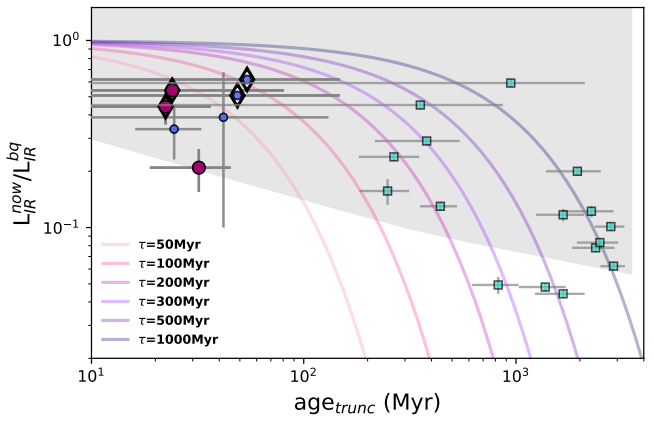
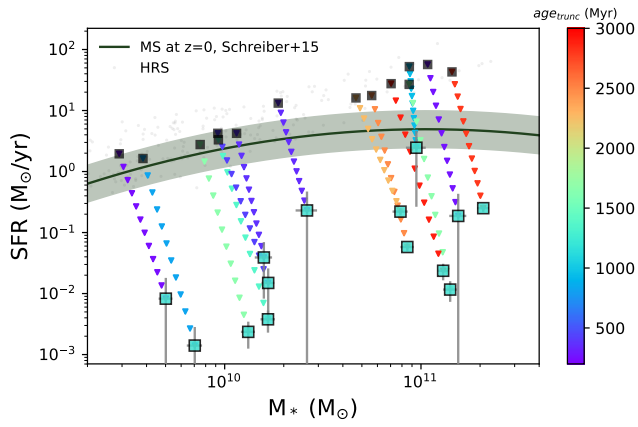
IR

age_n

Figure 7

L_{IR}^{bq}
ref L_{IR}

τ



$\tau = 50 \text{ Myr}$
 $\tau = 100 \text{ Myr}$
 $\tau = 200 \text{ Myr}$
 $\tau = 300 \text{ Myr}$
 $\tau = 500 \text{ Myr}$
 $\tau = 1000 \text{ Myr}$
 $\tau = \text{age}_n$

...
 $\sim 0.1 \text{ Myr}$
 ...
 $\tau = 50 \text{ Myr}$
 $\tau = 100 \text{ Myr}$
 $\tau = 200 \text{ Myr}$
 $\tau = 300 \text{ Myr}$
 $\tau = 500 \text{ Myr}$
 $\tau = 1000 \text{ Myr}$
 $\tau = \text{age}_n$

7. Discussion

...
 $\tau = 50 \text{ Myr}$
 $\tau = 100 \text{ Myr}$
 $\tau = 200 \text{ Myr}$
 $\tau = 300 \text{ Myr}$
 $\tau = 500 \text{ Myr}$
 $\tau = 1000 \text{ Myr}$
 $\tau = \text{age}_n$

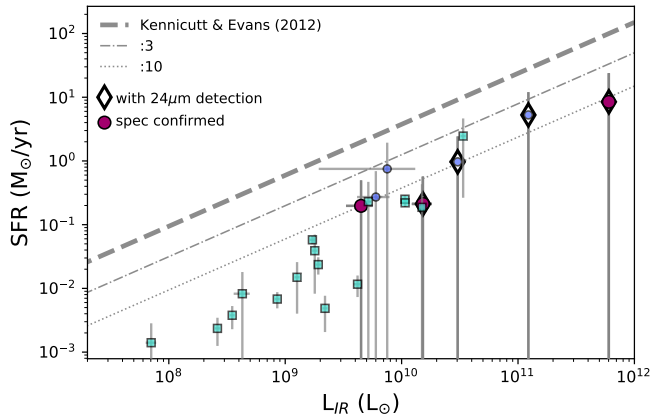
$L_{IR}^{now} / L_{IR}^{trunc}$
 $\tau = 50 \text{ Myr}$
 $\tau = 100 \text{ Myr}$
 $\tau = 200 \text{ Myr}$
 $\tau = 300 \text{ Myr}$
 $\tau = 500 \text{ Myr}$
 $\tau = 1000 \text{ Myr}$
 $\tau = \text{age}_n$

L_{IR} / M_*
 $\tau = 50 \text{ Myr}$
 $\tau = 100 \text{ Myr}$
 $\tau = 200 \text{ Myr}$
 $\tau = 300 \text{ Myr}$
 $\tau = 500 \text{ Myr}$
 $\tau = 1000 \text{ Myr}$
 $\tau = \text{age}_n$

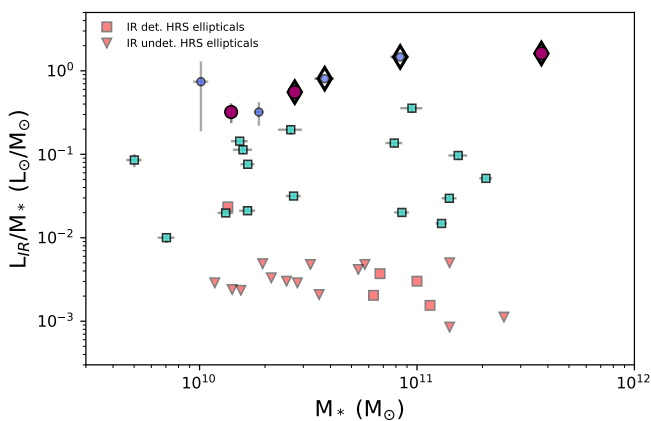
IR luminosity

(eg $10^8 L_\odot$)
IR luminosity
LIR
fraction

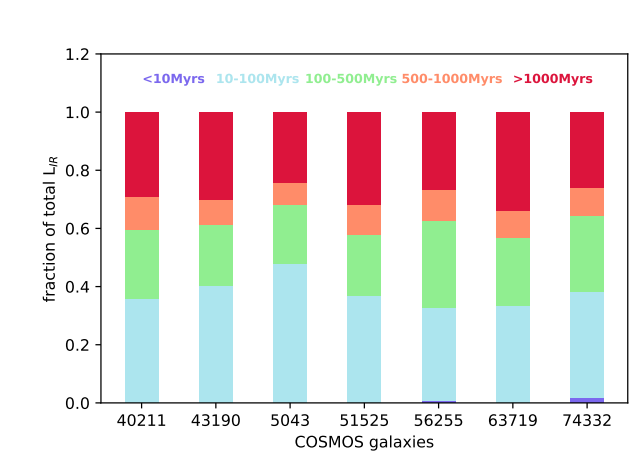
IR L_{IR}
fraction



IR luminosity
fraction



IR luminosity
fraction



IR luminosity

IR luminosity

IR luminosity

$\frac{L_{IR}^{now}}{L_{IR}^{bq}}$

$\frac{L_{IR}^{now}}{L_{IR}^{bq}}$

$\frac{L_{IR}^{now}}{L_{IR}^{bq}}$

IR luminosity

fraction

fraction

fraction

dust τ_{IR}

$\frac{d}{dt} \ln \left(\frac{L}{L_{\odot}} \right) = \frac{L}{L_{\odot}} \left(\frac{1}{\tau} - \frac{1}{\tau_{\text{H}}} \right)$
 where τ is the main-sequence lifetime and τ_{H} is the hydrogen burning time.

$\tau_{\text{H}} \approx 10^{10} \text{ yr}$

8. Conclusions

We have shown that the observed evolution of the $\text{H}\alpha$ emission line in the H II region of the $\text{NGC 1893$ cluster is consistent with the predictions of the theory of the evolution of H II regions.

$$\frac{d}{dt} \ln \left(\frac{L}{L_{\odot}} \right) = \frac{L}{L_{\odot}} \left(\frac{1}{\tau} - \frac{1}{\tau_{\text{H}}} \right)$$

The observed evolution of the $\text{H}\alpha$ emission line in the H II region of the NGC 1893 cluster is consistent with the predictions of the theory of the evolution of H II regions.

$\tau_{\text{H}} \approx 10^{10} \text{ yr}$

$\frac{d}{dt} \ln \left(\frac{L}{L_{\odot}} \right) = \frac{L}{L_{\odot}} \left(\frac{1}{\tau} - \frac{1}{\tau_{\text{H}}} \right)$

The observed evolution of the $\text{H}\alpha$ emission line in the H II region of the NGC 1893 cluster is consistent with the predictions of the theory of the evolution of H II regions.

$\tau_{\text{H}} \approx 10^{10} \text{ yr}$

The observed evolution of the $\text{H}\alpha$ emission line in the H II region of the NGC 1893 cluster is consistent with the predictions of the theory of the evolution of H II regions.

$\tau_{\text{H}} \approx 10^{10} \text{ yr}$

The observed evolution of the $\text{H}\alpha$ emission line in the H II region of the NGC 1893 cluster is consistent with the predictions of the theory of the evolution of H II regions.

$\tau_{\text{H}} \approx 10^{10} \text{ yr}$

The observed evolution of the $\text{H}\alpha$ emission line in the H II region of the NGC 1893 cluster is consistent with the predictions of the theory of the evolution of H II regions.

$\tau_{\text{H}} \approx 10^{10} \text{ yr}$

Herschel

$z < 1$

IR

IR

IR

IR

IR

IR

IR/M*

IR

The observed evolution of the $\text{H}\alpha$ emission line in the H II region of the NGC 1893 cluster is consistent with the predictions of the theory of the evolution of H II regions.

Acknowledgements. I thank the referee for his/her helpful comments.

References

AGUL, H.P. & FLORES, A. 1998
 BAL, E.D., III, & STANFORD, E.B. 1988
 BAL, E.D. & STANFORD, E.B. 1991
 BAL, E.D. 1995
 BAL, E.D. & STANFORD, E.B. 1998
 BAL, E.D., STANFORD, E.B. & STANFORD, E.B. 1999
 BAL, E.D. & STANFORD, E.B. 2000
 BAL, E.D., STANFORD, E.B. & STANFORD, E.B. 2001
 BAL, E.D., STANFORD, E.B. & STANFORD, E.B. 2002
 BAL, E.D., STANFORD, E.B. & STANFORD, E.B. 2003
 BAL, E.D., STANFORD, E.B. & STANFORD, E.B. 2004
 BAL, E.D., STANFORD, E.B. & STANFORD, E.B. 2005
 BAL, E.D., STANFORD, E.B. & STANFORD, E.B. 2006
 BAL, E.D., STANFORD, E.B. & STANFORD, E.B. 2007
 BAL, E.D., STANFORD, E.B. & STANFORD, E.B. 2008
 BAL, E.D., STANFORD, E.B. & STANFORD, E.B. 2009
 BAL, E.D., STANFORD, E.B. & STANFORD, E.B. 2010
 BAL, E.D., STANFORD, E.B. & STANFORD, E.B. 2011
 BAL, E.D., STANFORD, E.B. & STANFORD, E.B. 2012
 BAL, E.D., STANFORD, E.B. & STANFORD, E.B. 2013
 BAL, E.D., STANFORD, E.B. & STANFORD, E.B. 2014
 BAL, E.D., STANFORD, E.B. & STANFORD, E.B. 2015
 BAL, E.D., STANFORD, E.B. & STANFORD, E.B. 2016
 BAL, E.D., STANFORD, E.B. & STANFORD, E.B. 2017
 BAL, E.D., STANFORD, E.B. & STANFORD, E.B. 2018
 BAL, E.D., STANFORD, E.B. & STANFORD, E.B. 2019
 BAL, E.D., STANFORD, E.B. & STANFORD, E.B. 2020
 BAL, E.D., STANFORD, E.B. & STANFORD, E.B. 2021
 BAL, E.D., STANFORD, E.B. & STANFORD, E.B. 2022
 BAL, E.D., STANFORD, E.B. & STANFORD, E.B. 2023
 BAL, E.D., STANFORD, E.B. & STANFORD, E.B. 2024
 BAL, E.D., STANFORD, E.B. & STANFORD, E.B. 2025

Figure 1

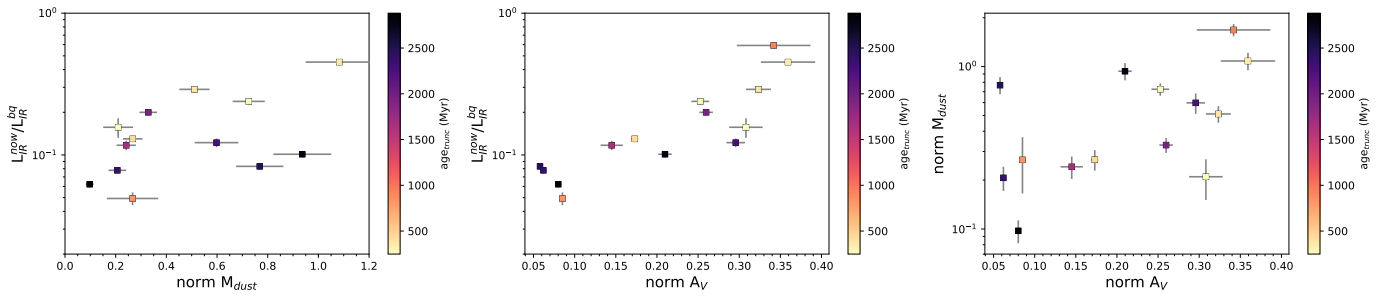


Figure 1
 Left: L_{IR}^{now}/L_{IR}^{bq} vs $norm M_{dust}$
 Middle: L_{IR}^{now}/L_{IR}^{bq} vs $norm A_V$
 Right: $norm M_{dust}$ vs $norm A_V$

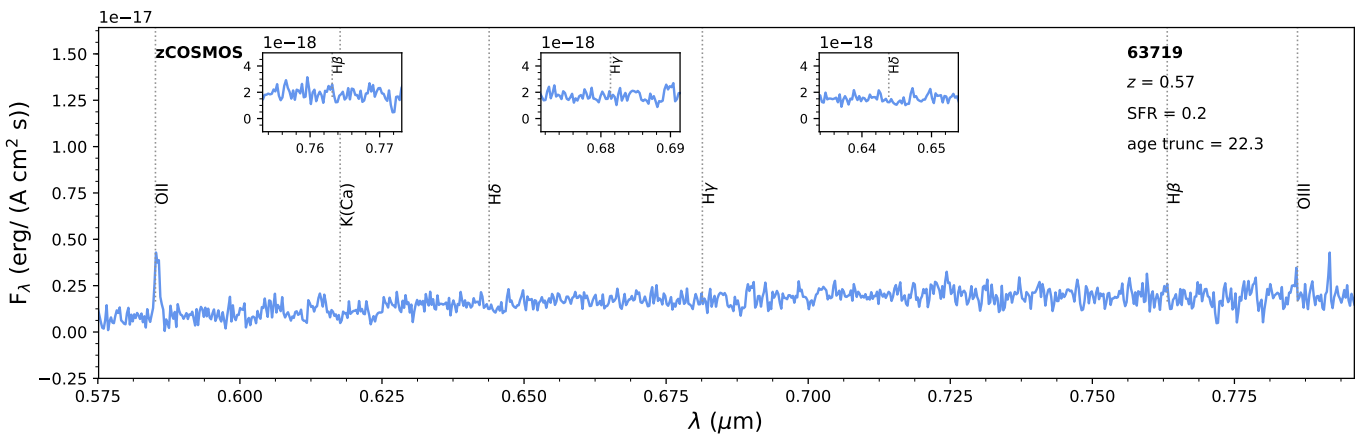
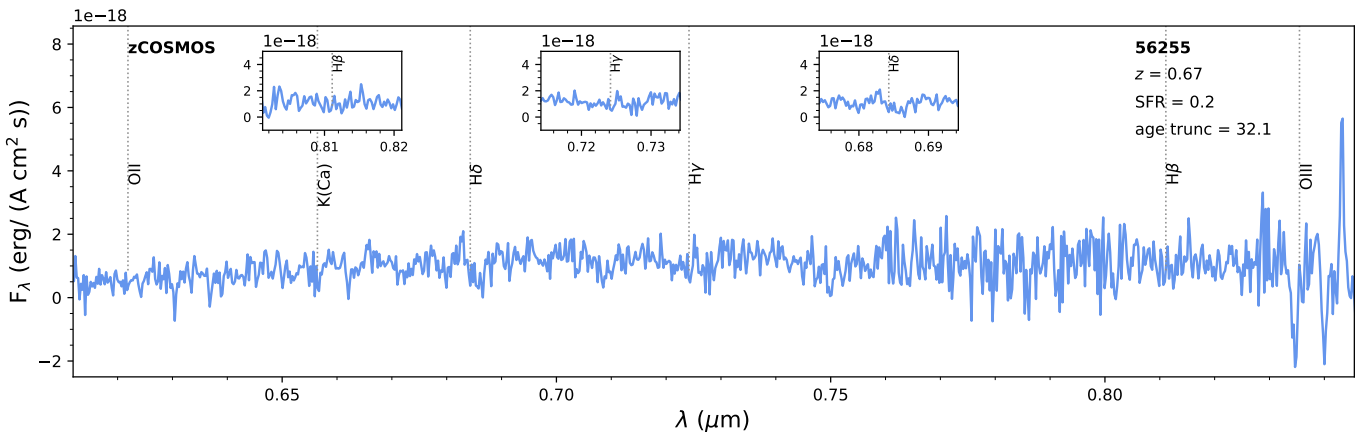
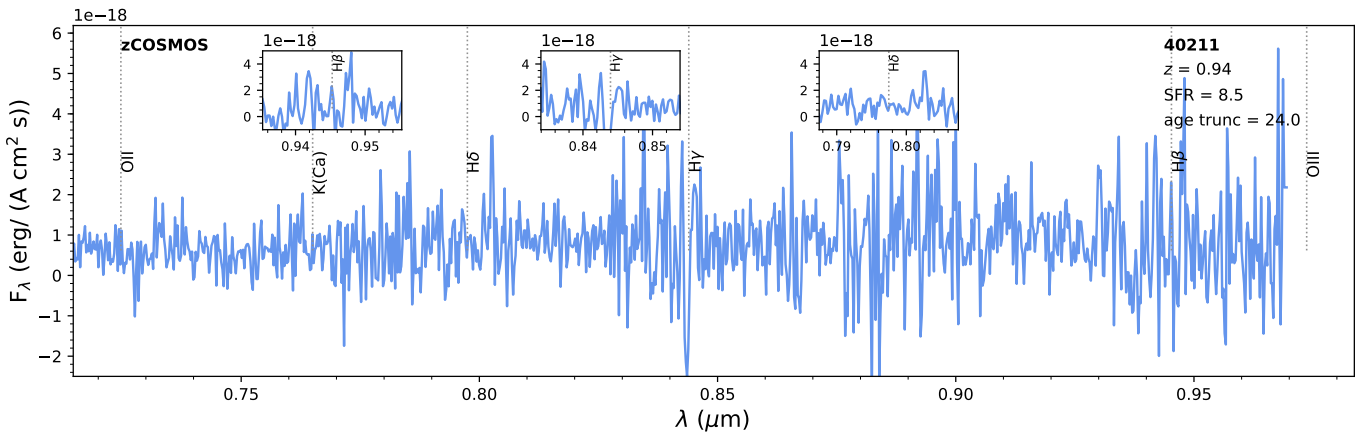
L_{IR}^{now}/L_{IR}^{bq}

age_{trunc}

- AKXZ & H083
- ALCC HL JMN th 0839
- AL9006
- BO th S th E th 0 & A9A
- IS th E th D th 0866
- KRC & EN th 08A93
- LC th HI, BO th 0866
- 022
- LSI, BVM th 0833
- MA th A th S th 0 & A6L
- MC th E th B th M th 0806
- NK th V th R th 0 & A0A
- NI-M th P th RCP & RJ th 086d
- 020
- NI & NI th 0809
- OK th B th ED th 08 M th 0872
- NI th C & NI th 0866
- OK th G th BI, th SM th 0866L
- NS th D th E th 0 & A99
- 0BD & ID éR th 0833
- ONE th CC & th H th 0802
- RY th CL, th E th 0806
- SI, th C & th CD th 0808
- UN th SE th SE th 0805
- BC th 0806
- th th 0801
- BB th S th 08, th 0860
- EG th E th BI, th 0809
- BF th E th D th 083L
- 0EE th 0826
- 0MT th E th B th M th 0809
- 0J th M & th C th 0826
- 0C th M th D th 0 & A5A
- 0C th M th R th 0 & A9A
- 0N th BK th H th 0808
- 0S th A th R th Y & th M th 0866
- th th 08
- 0M th L th 08, th SA th 0833
- 0M th CC th R th 0808
- 0J th S th CL, th PL & th D th 08A
- 25
- 0S th BA th CM th 0802
- 0S th J th C & th N th 0800
- 0AR th RF th K th V th 0808
- 0P th M th L th 0806
- th D th K th V th éI, 0C & th N th 08
- 0
- th M th 0808
- th M th 08 & th E th 0827
- th E th L th SI, th G & th I th 0833
- th KE th M th J, th 0800
- th S th F th N th M th 0826
- th A th A th N th 0802

Appendix A: Optical spectra of the candidates

zCOSMOS



zCOSMOS

β , $H\gamma$, $H\delta$